Int. J. Solids Structures, 1970, Vol 6, pp 909 to 932. Pergamon Press. Printed in Great Britain

BUCKLING OF RETICULATED SHELL STRUCTURES†

STEVEN E. FORMAN and JOHN W. HUTCHINSON

Harvard University,
Cambridge, Massachusetts

Abstract—Buckling analyses of several reticulated shell structures are carried out using both an approximate equivalent shell analysis and a discrete analysis which is essentially exact. The structures considered are: an infinite reticulated beam under axial compression and resting at equally spaced intervals on elastic springs; a shallow section of a reticulated sphere with an equilateral triangle grid subject to normal loading; and an infinite reticulated cylindrical shell with an equilateral triangle grid subject to axial compression. The discrete analysis is used to evaluate the accuracy of the predictions of the equivalent shell analysis. The buckling load computed on the basis of the equivalent shell analysis is nonconservative when a characteristic wavelength of the buckling deformation is on the order of the member length or the axial load in a member at buckling is on the order of the Euler buckling load of a simply supported column. The effect on the buckling load of reducing the rigidity of the joints is investigated for both the beam-spring model and the reticulated spherical shell. Finally, the importance of the discrete analysis is illustrated by the determination of the optimum properties of a shallow section of a reticulated sphere subject to a prescribed normal loading and designed against buckling.

INTRODUCTION

A COMMON method of analyzing the buckling of a reticulated plate or shell structure is to approximate it by an equivalent continuous plate or shell and to make use of the large number of results which have already accumulated for such structures. The history and development of this approximate type of analysis are discussed extensively in a paper by Wright [1], where effective stretching and bending properties for a number of reticulated shell surface patterns are derived and used to introduce equivalent shell structures. The validity of the equivalent plate approach to reticulated plates can be assessed from discrete calculations of Renton [2–4] and Wah [5] for bending of reticulated plates under normal load and by Wah [6] for buckling under inplane loads. In general, the equivalent plate predictions for buckling are accurate so long as there is a sufficiently large number of members included in a distance comparable to the characteristic buckling wavelength, which for plates is, in turn, usually comparable to the shortest inplane dimension.

Applicability of an equivalent shell theory of buckling to reticulated shells is more difficult to assess. For shells, the characteristic buckle wavelength can be on the order of $\sqrt{(Rt)}$, where R is a radius of curvature and t is an effective thickness. Certainly this length must exceed the member length if an equivalent shell theory is to be used. The validity of the continuous approximation is also limited by the reduction in stiffness of the members in a reticulated shell when the axial loads in the members are close to the Euler buckling load of the individual beams.

In this paper the buckling of reticulated structures will be analyzed using an exact discrete formulation which accounts for the behavior of the individual beams. The simple,

† This work was supported in part by the National Aeronautics and Space Administration under Grant NGL 22-007-012, and by the Division of Engineering and Applied Physics, Harvard University.

yet fundamental, reticulated shell structures considered here consist of a plane or curved surface composed of a single layer of straight beams arranged in some repeating pattern. Figure 1 illustrates four such reticulated shell structures which utilize the equilateral triangle as a surface element. Several problems of varying complexity will be investigated and the predictions based on the discrete analysis will be compared with those obtained from the equivalent shell analysis with the aim of determining the range of validity of this latter approximate theory.

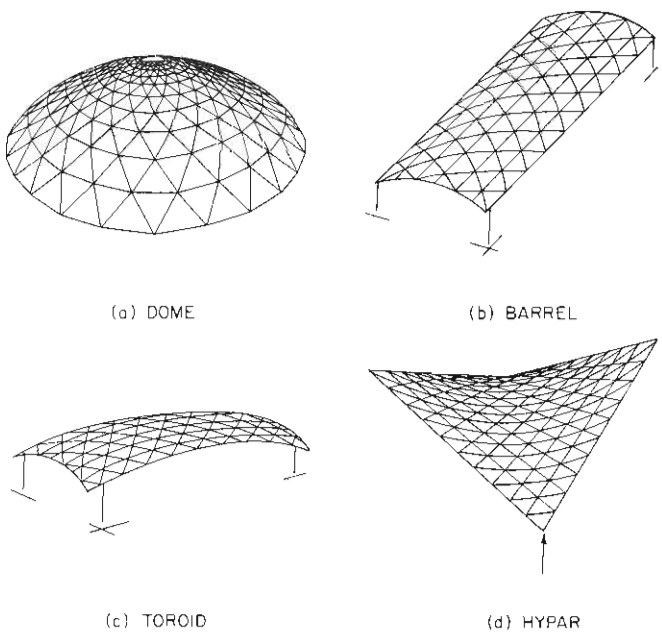

FIG. 1. Examples of reticulated shells.

The first and simplest buckling problem which will be used to illustrate the method of analysis is a variation of a problem which is often used to model shell buckling. It is the buckling of an axially compressed infinite reticulated beam which rests at equally spaced intervals on linear elastic springs. Predictions for both rigid and non-rigid joints connecting the member beams are obtained. The second problem examined is the buckling of a shallow section of a reticulated sphere with an equilateral triangle grid which is subject to equal inward loads at each joint. Again the separate cases of rigid and non-rigid joints will be considered. The final problem treated is the buckling of an infinite reticulated cylindrical shell, with an equilateral triangle grid with rigid joints, subject to an axially compressive loading.

To further illustrate the importance of a discrete analysis, optimum properties (i.e. member length, stiffness and weight) are found for a shallow section of a reticulated sphere of a given radius, subject to a prescribed effective external pressure and possessing an equilateral triangle grid with rigid joints.

BUCKLING ANALYSIS OF A MODEL RETICULATED STRUCTURE

Consider an infinite reticulated beam under axial compression P_a, resting at equally spaced intervals on elastic springs as depicted in Fig. 2(a). Each spring exerts a restoring force Cw on the beam, where C is the elastic spring constant and w is the normal deflection of the beam at the spring. Adjoining beams are pinned at the springs and relative rotation is restrained by a rotational spring which is introduced to model the effects of non-rigid joints. The moment exerted by one beam on its adjacent neighbor (transmitted by the torsional spring) is $k\theta^*$ where k is the spring constant and θ^* is the relative rotation of the adjoining beam ends. Of special interest will be the case in which the rotational spring constant is infinite and the beams are rigidly connected to form an infinite beam.

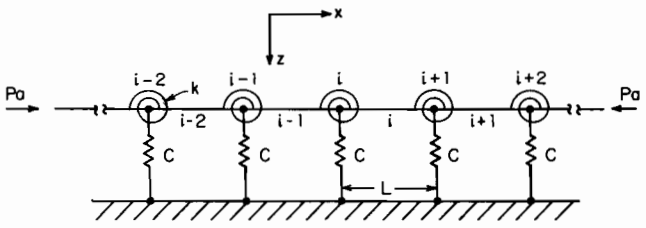

FIG. 2(a). Infinite reticulated beam under axial compression resting on equally spaced springs.

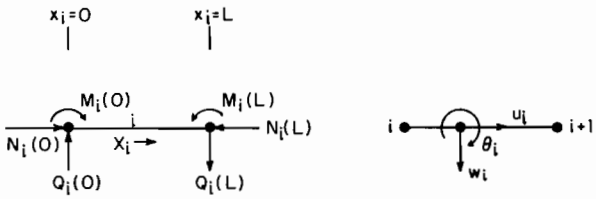

FIG. 2(b). Sign conventions for forces, moments, deflections and rotations of the ith member.

The equivalent beam analysis of the model reticulated structure with rigid joints

If the characteristic wavelength of the buckling mode is long compared to the distance between springs the effect of the individual springs can be approximated by smearing them out and replacing them by an elastic foundation. This beam-spring system is characterized by the well-known differential equation for a beam on a continuous elastic foundation subject to axial load P_a [7],

$$EI\frac{d^4w}{dx^4}+P_a\frac{d^2w}{dx^2}+\frac{C}{L}w=0 \tag{1}$$

where x is the axial coordinate, E is Young's Modulus, I is the moment of inertia of the beam cross-section, and C/L is the effective spring constant per unit length of the elastic foundation.

Buckling of the beam is associated with bifurcation from the initially straight configuration. The eigenfunctions and eigenvalues of this problem are respectively

$$w = \sin \mu \frac{x}{L} \tag{2}$$

and

$$P_a L^2/EI = \mu^2 + (CL^3/EI)/\mu^2. \tag{3}$$

It is now convenient to introduce the dimensionless parameters $P = (P_a L^2/EI)^{\frac{1}{2}}$ and $C^* = (CL^3/EI)$. The buckling load P_c, i.e. the minimum eigenvalue, and the associated wave number μ_c are

$$P_c = (4C^*)^{\frac{1}{2}}, \qquad \mu_c = (C^*)^{\frac{1}{2}}. \tag{4}$$

These predictions will be checked against the exact results obtained next. Tentatively, we expect these formulas to be valid as long as the axial load in the members is sufficiently less than the Euler buckling load for a simply supported column (i.e. $C^* < \pi^4/4$) and the wavelength of the buckling mode is large compared to the member length.

Discrete analysis of the model reticulated structure

The discrete analysis proceeds from a variational statement of the principle of virtual work. If it is assumed that buckling occurs only in the x–z plane of Fig. 2(a), then the principle of virtual work can be stated as follows

$$\sum_i \int_0^L (-N_i \delta\varepsilon_i + M_i \delta\kappa_i)\, \mathrm{d}x + \sum_i C\underline{w}_i \delta\underline{w}_i + \sum_i k\theta_i^* \delta\theta_i^* = EVW \text{ of applied loads} \tag{5}$$

where N_i is the axial load, ε_i the axial strain, M_i the moment, κ_i the curvature and x the axial measure of distance, all for the ith member, and $\underline{w}_i$ is the normal deflection of the ith joint†. The joints and members are numbered in Fig. 2(a) such that the ith joint precedes the ith member. Since it is anticipated that the solution found will possess a certain periodicity along the beam, the variational statement above is written for a representative length of the structure.

The strain measures of small-rotation beam theory are entirely adequate for the present buckling analysis. For buckling in the x–z plane, they are

$$\varepsilon_i = \frac{\mathrm{d}u_i}{\mathrm{d}x} + \frac{1}{2}\left(\frac{\mathrm{d}w_i}{\mathrm{d}x}\right)^2 \tag{6}$$

$$\kappa_i = -\frac{\mathrm{d}^2 w_i}{\mathrm{d}x^2} \tag{7}$$

† The bars underlining the joint displacements and rotations (e.g. $\underline{w}_i$) are used to distinguish them from the displacements and rotations of points on the neutral axis of the members (e.g. w_i)

where u_i and w_i are the axial and normal displacements respectively of the ith member. The slope of the deformed ith member at any point along its neutral axis θ_i, the change in slope across the ith joint θ_i^*, and the average slope at the ith joint $\underline{\theta}_i$ are given by

$$\theta_i = \frac{\mathrm{d}w_i}{\mathrm{d}x}, \qquad \theta_i^* = \theta_i(0) - \theta_{i-1}(L), \qquad \underline{\theta}_i = [\theta_i(0) + \theta_{i-1}(L)]/2 \tag{8}$$

and the transverse shear force in the ith member is

$$Q_i = \frac{\mathrm{d}M_i}{\mathrm{d}x}. \tag{9}$$

All the beam forces, moments, displacements and rotations are shown in Fig. 2(b) along with their respective sign conventions.

A restatement of the principle of virtual work, using the strain measures and definitions given above, following appropriate integration by parts leads to the member equilibrium equations

$$N_{i,x} = 0; \qquad M_{i,xx} - (N_i w_{i,x})_{,x} = 0 \tag{10}$$

where $(\,)_{,x} \equiv [\mathrm{d}(\,)/\mathrm{d}x]$ and the joint equilibrium equations

$$\begin{aligned} N_{i-1}(L) - N_i(0) &= 0 \\ [N_i(0)\theta_i(0) - N_{i-1}(L)\theta_{i-1}(L)] + [Q_{i-1}(L) - Q_i(0)] + C\underline{w}_i &= 0 \\ M_{i-1}(L) - M_i(0) &= 0 \\ \frac{1}{2k}[M_i(0) + M_{i-1}(L)] + \theta_i^* &= 0. \end{aligned} \tag{11}$$

To investigate bifurcation from the initially straight configuration, perturbation series are developed about the pre-buckling state in the usual way i.e. $N_i(0) = P_a + \xi N_i^{(1)}(0) + \ldots$, $\underline{w}_i = \xi \underline{w}_i^{(1)} + \ldots$, etc. where ξ is the perturbation parameter. These expansions lead to the following linear algebraic problem which consists of the member equations

$$N_{i,x}^{(1)} = 0; \qquad M_{i,xx}^{(1)} - P_a w_{i,xx}^{(1)} = 0 \tag{12}$$

and the joint equilibrium equations

$$\begin{aligned} P_a\theta_i^{*(1)} + Q_{i-1}^{(1)}(L) - Q_i^{(1)}(0) + C\underline{w}_i^{(1)} &= 0 \\ M_{i-1}^{(1)}(L) - M_i^{(1)}(0) &= 0 \\ \frac{1}{2k}[M_{i-1}^{(1)}(L) + M_i^{(1)}(0)] + \theta_i^{*(1)} &= 0. \end{aligned} \tag{13}$$

Equations (12) yield slope-deflection equations which relate the forces and moments at the ends of the ith member to the rotations and deflections at the ends. They are defined

consistent with the sign convention of Fig. 2(b) and are given by

$$
\begin{aligned}
N_i^{(1)}(0) &= N_i^{(1)}(L) = -\frac{EA}{L}[u_i^{(1)}(L)-u_i^{(1)}(0)] \\
M_i^{(1)}(0) &= \frac{2EI}{L}\left[2C_{10}\theta_i^{(1)}(0)+C_{20}\theta_i^{(1)}(L)-\frac{3C_{30}}{L}(w_i^{(1)}(L)-w_i^{(1)}(0))\right] \\
M_i^{(1)}(L) &= -\frac{2EI}{L}\left[2C_{10}\theta_i^{(1)}(L)+C_{20}\theta_i^{(1)}(0)-\frac{3C_{30}}{L}(w_i^{(1)}(L)-w_i^{(1)}(0))\right] \\
Q_i^{(1)}(0) &= Q_i^{(1)}(L) = -\frac{6EI}{L^2}\left[C_{30}(\theta_i^{(1)}(0)+\theta_i^{(1)}(L))-\frac{2C_{40}}{L}(w_i^{(1)}(L)-w_i^{(1)}(0))\right]
\end{aligned}
\tag{14}
$$

where A is the member cross-sectional area and C_{10}, C_{20}, C_{30} and C_{40} are the well known stability functions [8–10] which are defined as follows

$$
C_{10} = \frac{P(\sin P - P\cos P)}{4(2-2\cos P - P\sin P)} \qquad C_{30} = \frac{P^2(1-\cos P)}{6(2-2\cos P - P\sin P)}
$$

$$
C_{20} = \frac{P(P-\sin P)}{2(2-2\cos P - P\sin P)} \qquad C_{40} = \frac{P^3\sin P}{12(2-2\cos P - P\sin P)}
$$

where P is the dimensionless load parameter used in the equivalent beam analysis, $(P_aL^2/EI)^{\frac{1}{2}}$.

The joint equilibrium equations are now converted into three finite difference equations in terms of slope quantities and deflections at the ith joint and the two joints adjacent to it. A considerable notational simplification of these equations is achieved by introducing the shifting operators of the calculus of finite differences [11, 12]—defined by $E_if_i = f_{i+1}$ and $E_i^{-1}f_i = f_{i-1}$. With these operators, the joint equilibrium equations are:

$$
\begin{aligned}
&[4C_{10}+C_{20}(E_i+E_i^{-1})]\theta_i^{(1)}-3C_{30}(E_i-E_i^{-1})\frac{w_i^{(1)}}{L}-\frac{C_{20}}{2}(E_i-E_i^{-1})\theta_i^{*(1)} = 0 \\
&C_{30}(E_i-E_i^{-1})\theta_i^{(1)}+\left(\frac{C^*}{6}-2C_{40}(E_i+E_i^{-1}-2)\right)\frac{w_i^{(1)}}{L}+\left(\frac{P^2}{6}+1-\frac{1}{2}(E_i+E_i^{-1})\right)\theta_i^{*(1)} = 0 \\
&C_{20}(E_i-E_i^{-1})\theta_i^{(1)}-3C_{30}(E_i+E_i^{-1}-2)\frac{w_i^{(1)}}{L}+\left(B+2C_{10}-\frac{C_{20}}{2}(E_i+E_i^{-1})\right)\theta_i^{*(1)} = 0
\end{aligned}
\tag{15}
$$

where $B = kL/EI$.

The case of rigid joints ($k = \infty$) is investigated first. With $\theta_i^* = 0$, equations (15) can be reduced to a single fourth order finite difference equation in terms of the joint displacements $w_i^{(1)}$:

$$
\left[\frac{3C_{30}^2(E_i-E_i^{-1})^2}{4C_{10}+C_{20}(E_i+E_i^{-1})}+\frac{C^*}{6}+2C_{40}(2-E_i-E_i^{-1})\right]w_i^{(1)} = 0. \tag{16}
$$

The eigensolutions associated with (16) are

$$
w_i^{(1)} = \sin \mu i \tag{17}
$$

where μ is the wave number, and the associated eigenvalue equation is

$$\frac{C^*}{6} - \frac{6C_{30}^2 \sin^2 \mu}{2C_{10} + C_{20} \cos \mu} + 4C_{40}(1 - \cos \mu) = 0 \tag{18}$$

or in the functional notation

$$F(P, \mu, C^*) = 0.$$

A straightforward numerical procedure has been applied to (18) to find the critical eigenvalues associated with buckling for fixed values of C^*.

A direct calculation, which will not be given here, demonstrates that when the axial load in a member is small compared to the Euler buckling load and the characteristic wavelength of the buckling mode is large compared to the member length the eigenvalue equation of discrete analysis reduces asymptotically to that of the equivalent beam analysis —equation (3).

In Fig. 3, the curve denoted by rigid joints is constructed by normalizing the buckling load predicted by discrete analysis by the prediction of equivalent-beam analysis—equation (4)—and plotting this ratio for given values of C^*. At $C^* = 10$, the critical axial load in a member predicted by equivalent-beam theory is 1 per cent higher than the exact value predicted by discrete analysis. Furthermore, at this value of C^* the exact load is 63 per cent of the Euler load and the buckle half-wavelength is 1·77 times the member length. However at $C^* = 25$, when the actual member load is 92 per cent of the Euler load and the buckle half-wavelength is 1·37 times the member length, the prediction of equivalent beam theory

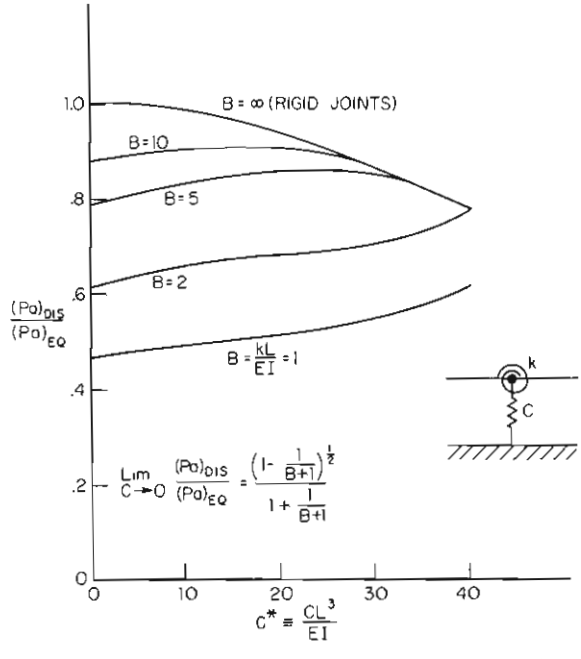

FIG. 3. Buckling of the beam-spring model (rigid and non-rigid joints).

is 10 per cent too high. For even larger values of C^* the predictions of the equivalent beam analysis grow increasingly more inaccurate. At $C^* = 4\pi^2$ it can be shown using the discrete analysis that the half-wavelength of buckling is exactly equal to the member length, i.e. $\mu_c = \pi$, and the axial member load is equal to the Euler load, i.e. $P_c = \pi$. Thus the beam-spring model buckles only between the springs. This problem was previously solved by Budiansky, Weinberger and Seide [13] using a somewhat different procedure than used here.

The equations for the case in which the joints are non-rigid can also be reduced to the form

$$\mathscr{L}(\underline{w}_i^{(1)}) = 0$$

where now $\mathscr{L}$ is a sixth order difference operator. The eigensolutions are again of the form of (17) and the eigenvalue equation is

$$C^* - 24C_{40}(\cos\mu - 1) + \frac{6C_{30}(\cos\mu - 1)[P^2 + 6(1-\cos\mu)]}{2C_{10} + B - C_{20}\cos\mu} - 12C_{30}\sin^2\mu\left(1 + \frac{C_{20}(\cos\mu - 1)}{2C_{10} + B - C_{20}\cos\mu}\right)\left(6C_{30} - \frac{C_{20}[P^2 + 6(1-\cos\mu]}{2C_{10} + B - C_{20}\cos\mu}\right) + \frac{}{2\left(2C_{10} + C_{20}\cos\mu - \frac{C_{20}^2\sin^2\mu}{2C_{10} + B - C_{20}\cos\mu}\right)} = 0 \quad (19)$$

or in functional notation

$$F(P, \mu, C^*, B) = 0.$$

The significance of the parameter B can be explained by considering a cantilever beam of bending stiffness EI and length L which is loaded at its free end by a transverse load S and supported at its other end by a rotational spring k. The deflection at the free end of this cantilever beam is

$$w = \frac{SL^3}{EI}\left(\frac{1}{3} + \frac{1}{B}\right).$$

When B is infinite, the beam is rigidly clamped and the deflection is due entirely to the bending of the beam. When, for example, $B = 3$, the deflection at the free end due to bending is the same as the contribution due to the rotation of the spring.

The critical eigenvalues predicted by the discrete analysis have again been normalized with respect to the predictions of equivalent beam theory with rigid joints [equation (4)], and this ratio has been plotted in Fig. 3 as a function of C^* for different values of B. When B is greater than about 25, the joints are effectively rigid. For smaller values of B, there is a marked departure from the discrete analysis with rigid joints and the non-rigid effect of the joints must be taken into account.

Equation (19) can be solved asymptotically when C^* is sufficiently small, that is, in the region where the wavelength of the buckling mode is large compared to the member lengths and the axial load in a member is small compared to the Euler load. A very simple formula results which clearly shows the effects of the non-rigid joints. This formula is

$$\lim_{c\to 0}\frac{(P_a)\ \text{discrete}}{(P_a)\ \text{equivalent-beam}} = \frac{[1 - 1/(B+1)]^{\frac{1}{2}}}{1 + 1/(B+1)}. \quad (20)$$

While this is an asymptotic equation, Fig. 3 shows that the normalized buckling load ratio does not change appreciably until C^* becomes larger than about 10. Therefore, (20) gives a reasonable estimate of the effects of non-rigid joints in the range where the equivalent theory is valid for the analysis of the beam-spring model with rigid joints.

BUCKLING ANALYSIS OF A SHALLOW SECTION OF A RETICULATED SPHERE UNDER NORMAL LOADING

In this section we consider a shallow section of a reticulated spherical shell with a repeating equilateral triangle grid which is loaded at each joint by an inward radial force F. The member length L is assumed to be very short compared to the characteristic dimension of the shallow section. Of course, such an equilateral triangular pattern must be distorted in certain regions to cover an entire sphere. Here, our focus is on a shallow section in which there is no distortion of the grid to first approximation. A classical buckling analysis of this shallow section is carried out using both an equivalent shell theory and a discrete theory. Consideration is restricted to member properties such that the reticulated shell is effectively very thin and therefore the buckle pattern is duplicated many times over the surface of the shallow section. This feature is exploited and only periodic shallow buckling modes are investigated. The constraining effects at the edge of the section or of the adjoining shell, if the section is regarded as part of a complete sphere, are not treated in detail. Our main concern is the discrete buckling behavior peculiar to the grid.

Equivalent shell analysis of the shallow spherical section with rigid joints

If the characteristic wavelengths of the buckling mode are long compared to the member lengths then the deformation of the segment can be modeled by replacing it by a continuous shell. The equivalent shell associated with the equilateral triangle grid shown in Fig. 4 is isotropic and its effective bending and stretching properties are [1, 14]

$$D_e = \frac{\sqrt{(3)}EI}{4L}\left(3+\frac{GJ}{EI}\right) \qquad (Et)_e = \frac{2AE}{\sqrt{(3)}L}$$
$$\nu_B^e = [(1-GJ/EI)/(3+GJ/EI)] \qquad \nu_S^e = \tfrac{1}{3} \tag{21}$$

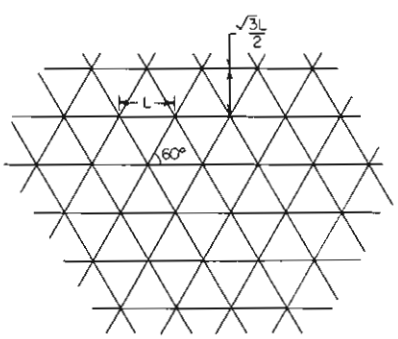

FIG. 4(a). Equilateral triangle grid.

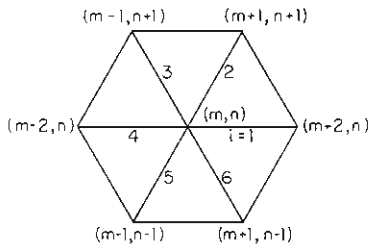

FIG. 4(b). Grid and member numbering systems—spherical section.

where EI is the flexural rigidity of a member (which in this study is taken to be the same about all bending axes), GJ is its torsional rigidity, EA is its axial stiffness, D_e and $(Et)_e$ are the bending and stretching stiffnesses, respectively, of the equivalent shell and ν_B^e and ν_S^e are the effective Poisson's ratios of the shell for bending and stretching.

The loading applied to the reticulated shell in the form of equal inward radial forces at each joint is replaced by a uniform pressure p over the equivalent shell where $p = 2F/\sqrt{(3)}L^2$. The critical buckling pressure for a complete spherical shell with the properties listed above is well known and is given by the equation

$$p_c = \frac{4}{R^2}[D_e(Et)_e]^{\frac{1}{2}} \tag{22}$$

Precisely this same value is obtained by a shallow shell analysis, in the spirit of that described above, which ignores the boundary conditions at the edge of the section. Shallow buckling modes of the form $w = (\sin \mu x)(\sin \nu y)$ are considered where w is the normal deflection and μ and ν are wave numbers associated with coordinates x and y in the surface [15]. The wavelengths characterizing such a buckle pattern are "short" and of the order of $\sqrt{(Rr_g)}$, where $r_g = \sqrt{(I/A)}$ is the radius of gyration of the member cross-section.

The pre-buckling load in each member is the same, P_a, and is related to the normal load at the joint F by $P_a = RF/3L$ where R is the radius of the sphere. Hence the value of the axial load in each member at buckling is

$$\left(\frac{P_a L^2}{EI}\right)_{\text{crit}} = \frac{L^2}{r_g R}\left[\frac{2}{3}\left\{3 + \frac{GJ}{EI}\right\}\right]^{\frac{1}{2}}. \tag{23}$$

As long as the parameter $L/\sqrt{(r_g R)}$ is sufficiently small, so that the member length is short compared to the buckle wavelength and so that the axial member load at buckling $(P_a L^2/EI)_{\text{crit}}$ is well below the Euler buckling load of a simply supported column (i.e. π^2), it can be expected that (23) gives a good approximation to the critical axial member load†. When the axial member load at buckling is of the order of or larger than the Euler load a discrete analysis is necessary to accurately predict the critical eigenvalues.

† At this stage of the discussion it is not obvious that the simple support Euler load, rather than the Euler load for a clamped–clamped column say, is the relevant cutoff for the equivalent theory. It turns out, however, that it is.

Discrete analysis of the shallow spherical section with rigid joints

In principle, the discrete analysis of a shallow reticulated spherical shell is similar to that carried out for the model reticulated structure: but it is considerably more lengthy and involved and it will be necessary to omit most of the algebraic details. Only the important details of the analysis and the results obtained will be given in this section.

The joint numbering system that is employed is shown in Fig. 4. The six members emanating from a joint are numbered 1–6 in the counterclockwise fashion shown, and a typical member of the group of six will be referred to as the ith member.

Deformation of the structure as a whole is characterized by specifying six quantities—three displacements and three rotations—at each joint. As shown in Fig. 5, these quantities are specified with respect to a tangent plane which passes through the undeflected joint and makes equal angles (i.e. $\alpha/2$) with all the undeflected members originating from the joint. Typically, at the (m, n)th joint $\underline{u}_{m,n}$ and $\underline{v}_{m,n}$ are the two orthogonal displacements tangent to the plane, $\underline{w}_{m,n}$ is the displacement normal to the plane (positive inward), $\underline{\gamma}_{m,n}$ and $\underline{\theta}_{m,n}$ are the rotations about the two axes in the plane and $\underline{\phi}_{m,n}$ is the rotation about the axis normal to the plane.

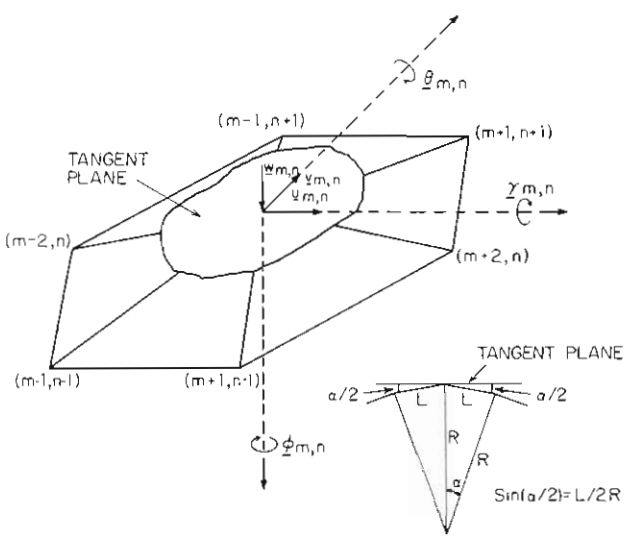

FIG. 5. Sign conventions for joint displacements and rotations—spherical section.

The displacements and rotations at the ends of the members, as defined with respect to a coordinate system along the length of the beam, are shown in Fig. 6 and are related to the joint displacements and rotations by

$$\begin{aligned} U &= AU_{m,n} \qquad \gamma = A\Gamma_{m,n} \\ V &= BU_{m,n} \qquad \Theta = B\Gamma_{m,n} \\ W &= CU_{m,n} \qquad \Phi = C\Gamma_{m,n} \end{aligned} \tag{24}$$

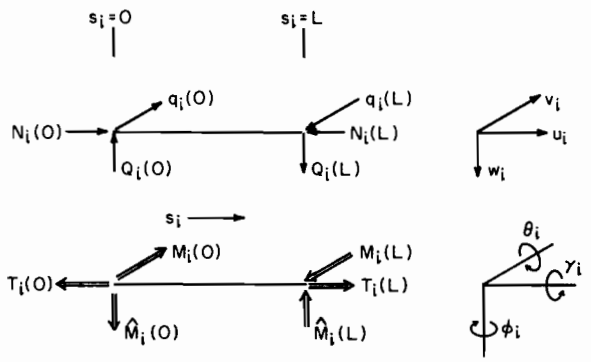

FIG. 6. Sign conventions for forces, moments, displacements and rotations of the ith member—spherical section.

where U, V, W, γ, Θ and Φ are (6×1) matrices containing the values of the member displacements and rotations at their ends terminating in the (m, n)th joint; $U_{m,n}$ and $\Gamma_{m,n}$ are (3×1) matrices containing the values of the deflections and rotations of the (m, n)th joint; and A, B and C are (6×3) matrices dependent on the geometric properties of the grid. The member displacement and rotation matrices are

$$U = [u_1(0), u_2(0), u_6(0), u_4(L), u_5(L), u_3(L)]$$

$$V = [v_1(0), v_2(0), v_6(0), v_4(L), v_5(L), v_3(L)], \text{ etc.}$$

and the joint displacement and rotation matrices are given as follows

$$U_{m,n} = [\underline{u}_{m,n}, \underline{v}_{m,n}, \underline{w}_{m,n}] \qquad \Gamma_{m,n} = [\underline{\gamma}_{m,n}, \underline{\theta}_{m,n}, \underline{\phi}_{m,n}]$$

and

$$A = \begin{bmatrix} a & 0 & b \\ a/2 & \sqrt{3}(a/2) & b \\ a/2 & -\sqrt{3}(a/2) & b \\ a & 0 & -b \\ a/2 & \sqrt{3}(a/2) & -b \\ a/2 & -\sqrt{3}(a/2) & -b \end{bmatrix} \qquad B = \begin{bmatrix} 0 & 1 & 0 \\ -\sqrt{3}/2 & 1/2 & 0 \\ \sqrt{3}/2 & 1/2 & 0 \\ 0 & 1 & 0 \\ -\sqrt{3}/2 & 1/2 & 0 \\ \sqrt{3}/2 & 1/2 & 0 \end{bmatrix}$$

$$C = \begin{bmatrix} -b & 0 & a \\ -b/2 & -\sqrt{3}(b/2) & a \\ -b/2 & \sqrt{3}(b/2) & a \\ b & 0 & a \\ b/2 & \sqrt{3}(b/2) & a \\ b/2 & -\sqrt{3}(b/2) & a \end{bmatrix}$$

where $a = \cos \alpha/2$ and $b = \sin \alpha/2$.

The variational statement of virtual work for a representative section of the shallow spherical shell is

$$\sum_{\text{members}} \int_0^L (-N_i\delta\varepsilon_i + M_i\delta\kappa_i + \hat{M}_i\delta\hat{\kappa}_i + T_i\delta\gamma_{i,s})\,\mathrm{d}s = \sum_m \sum_n F\delta\underline{w}_{m,n} \tag{25}$$

where N_i and ε_i are the compressive axial load and the axial strain; (M_i, κ_i) and $(\hat{M}_i, \hat{\kappa}_i)$ are the bending moments and curvatures about the two orthogonal bending axes; T_i and $\gamma_{i,s}$ are the twisting moment and twist per unit length; and s is the axial measure of distance, all for the ith member. As stated previously F is the inward radial load applied to a joint and $\underline{w}_{m,n}$ is the inward radial deflection of the joint.

The strain measures of small rotation theory, which are again adequate for the shallow modes anticipated, are given in terms of the deflections related to the coordinate system along the ith beam:

$$\begin{aligned} \varepsilon_i &= u_{i,s} + \tfrac{1}{2}(w_{i,s})^2 + \tfrac{1}{2}(v_{i,s})^2 \\ \kappa_i &= -w_{i,ss} \qquad \hat{\kappa}_i = v_{i,ss} \end{aligned} \tag{26}$$

where u_i, v_i and w_i are the axial, lateral and radial displacements respectively of the ith member. The slopes of the deformed ith member are given by

$$\theta_i = w_{i,s} \qquad \phi_i = -v_{i,s} \tag{27}$$

and the transverse shear forces acting on the ith member are

$$Q_i = M_{i,s} \qquad \hat{Q}_i = \hat{M}_{i,s}. \tag{28}$$

The sign conventions for all these quantities are shown in Fig. 6.

Now, as in the case of the model problem, a set of member equations and joint equilibrium equations can be found from the principle of virtual work. The pre-buckling state of the sphere under the loading prescribed is a simple one in which the axial load is the same in all members and is related to the applied loads by the relation $P_a = RF/3L$. Since buckling of the structure is associated with a bifurcation from the pre-buckling state, all force and displacement quantities will be expanded in perturbation series about it just as in the beam model analysis. In order to avoid a cumbersome notation, the superscripts indicating the first order buckling quantities of the perturbation series have been deleted, and all quantities except the pre-buckling term P_a should be thought of as perturbed quantities. The resulting linear eigenvalue problem consists of the member equations

$$\begin{aligned} N_{i,s} = 0 \qquad T_{i,s} &= 0 \\ M_{i,ss} - P_a w_{i,ss} &= 0 \\ \hat{M}_{i,ss} + P_a v_{i,ss} &= 0 \end{aligned} \tag{29}$$

and the 6 equations of equilibrium for a typical joint:

$$(N_1-N_4)\cos\frac{\alpha}{2}+[Q_1(0)+Q_4(L)]\sin\frac{\alpha}{2}+\frac{1}{2}(N_2-N_5)\cos\frac{\alpha}{2}+\frac{1}{2}[Q_2(0)+Q_5(L)]\sin\frac{\alpha}{2}$$
$$+\frac{\sqrt{3}}{2}[\hat{Q}_5(L)-\hat{Q}_2(0)]+\frac{1}{2}(N_6-N_3)\cos\frac{\alpha}{2}+\frac{1}{2}[Q_3(L)+Q_6(0)]\sin\frac{\alpha}{2}$$
$$+\frac{\sqrt{3}}{2}[\hat{Q}_6(0)-\hat{Q}_3(L)]-6P_a\theta_{m,n}\sin\frac{\alpha}{2}=0$$

$$[\hat{Q}_1(0)-\hat{Q}_4(L)]+\frac{\sqrt{3}}{2}(N_2-N_5)\cos\frac{\alpha}{2}+\frac{\sqrt{3}}{2}[Q_2(0)+Q_5(L)]\sin\frac{\alpha}{2}$$
$$+\frac{1}{2}[\hat{Q}_2(0)-\hat{Q}_5(L)]+\frac{\sqrt{3}}{2}(N_3-N_6)\cos\frac{\alpha}{2}-\frac{\sqrt{3}}{2}[Q_6(0)+Q_3(L)]\sin\frac{\alpha}{2}$$
$$+\frac{1}{2}[\hat{Q}_6(0)-\hat{Q}_3(L)]+6P_a\gamma_{m,n}\sin\frac{\alpha}{2}=0$$

$$(N_1+N_4)\sin\frac{\alpha}{2}+[Q_4(L)-Q_1(0)]\cos\frac{\alpha}{2}+(N_2+N_5)\sin\frac{\alpha}{2}$$
$$+[Q_5(L)-Q_2(0)]\cos\frac{\alpha}{2}+(N_6+N_3)\sin\frac{\alpha}{2}+[Q_3(L)-Q_6(0)]\cos\frac{\alpha}{2}=0$$

$$[M_1(0)-M_4(L)]+\frac{\sqrt{3}}{2}(T_5-T_2)\cos\frac{\alpha}{2}+\frac{1}{2}[M_2(0)-M_5(L)]-\frac{\sqrt{3}}{2}[\hat{M}_2(0)+\hat{M}_5(L)]\sin\frac{\alpha}{2}$$
$$+\frac{\sqrt{3}}{2}(T_6-T_3)\cos\frac{\alpha}{2}+\frac{1}{2}[M_6(0)-M_3(L)]+\frac{\sqrt{3}}{2}[\hat{M}_6(0)+\hat{M}_3(L)]\sin\frac{\alpha}{2}=0$$

$$(T_4-T_1)\cos\frac{\alpha}{2}-[\hat{M}_4(L)+\hat{M}_1(0)]\sin\frac{\alpha}{2}+\frac{1}{2}(T_5-T_2)\cos\frac{\alpha}{2}+\frac{\sqrt{3}}{2}[M_5(L)-M_2(0)]$$
$$-\frac{1}{2}[\hat{M}_2(0)+\hat{M}_5(L)]\sin\frac{\alpha}{2}+\frac{1}{2}(T_3-T_6)\cos\frac{\alpha}{2}+\frac{\sqrt{3}}{2}[M_6(0)-M_3(L)]$$
$$-\frac{1}{2}[\hat{M}_6(0)+\hat{M}_3(L)]\sin\frac{\alpha}{2}=0$$

$$-(T_1+T_4)\sin\frac{\alpha}{2}+[\hat{M}_1(0)-\hat{M}_4(L)]\cos\frac{\alpha}{2}-(T_2+T_5)\sin\frac{\alpha}{2}$$
$$+[\hat{M}_2(0)-\hat{M}_5(L)]\cos\frac{\alpha}{2}-(T_3+T_6)\sin\frac{\alpha}{2}+[\hat{M}_6(0)-\hat{M}_3(L)]\cos\frac{\alpha}{2}=0. \tag{30}$$

The above set of equations is completed with the addition of the stress–strain relations

$$\begin{aligned} N_i &= -AE\varepsilon_i \qquad & T_i &= GJ\gamma_{i,s} \\ M_i &= EI\kappa_i \qquad & \hat{M}_i &= EI\hat{\kappa}_i \end{aligned} \tag{31}$$

where, as previously stated, the bending stiffness EI is taken to be constant about all bending axes. The slope deflection equations are the same as those given by equations (14) together with the additional relations:

$$\begin{aligned} T_i(0) &= T_i(L) = \frac{GJ}{L}[\gamma_i(L)-\gamma_i(0)] \\ \hat{M}_i(0) &= \frac{2EI}{L}\left[2C_{10}\phi_i(0)+C_{20}\phi_i(L)+\frac{3C_{30}}{L}[v_i(L)-v_i(0)]\right] \\ \hat{M}_i(L) &= -\frac{2EI}{L}\left[2C_{10}\phi_i(L)+C_{20}\phi_i(0)+\frac{3C_{30}}{L}[v_i(L)-v_i(0)]\right] \\ \hat{Q}_i(0) &= \hat{Q}_i(L) = -\frac{6EI}{L^2}\left[C_{30}[\phi_i(0)+\phi_i(L)]+\frac{2C_{40}}{L}[v_i(L)-v_i(0)]\right]. \end{aligned} \tag{32}$$

These quantities are consistent with the sign convention of Fig. 6.

It remains to express the joint equilibrium equations in terms of the joint displacements and rotations, and this is accomplished with the aid of the slope–deflection equations. This step in the analysis is lengthy, but straightforward, and the algebraic effort is reduced with the use of finite difference operators. The results of this computation are six finite difference equations in terms of the displacements and rotations of the (m, n)th joint and the six joints adjacent to it. By expressing five of the displacement and rotation quantities in terms of the radial displacements $\underline{w}_{m,n}$, these six equations can be reduced to one finite difference equation in terms of normal joint displacements alone. Symbolically,

$$\mathscr{L}\underline{w}_{m,n} = 0 \tag{33}$$

where $\mathscr{L}$ is a 12th order finite difference operator and is omitted here in the interest of brevity.

The above finite difference equation admits periodic eigensolutions in the form

$$\underline{w}_{m,n} = \sin \mu m \sin \nu n \tag{34}$$

where μ and ν are the wave numbers associated with the characteristic buckling wavelengths. In functional notation the eigenvalue equation associated with this choice is of the form

$$\hat{Q}_i(0) = \hat{Q}_i(L) = -\frac{P_{cr}L^2}{L^2}\left[C_{30}[\phi_i(0)+\phi_i(L)]+\frac{2C_{40}}{L}[v_i(L)-v_i(0)]\right].$$

These quantities are consistent with the sign convention of Fig. 6.

It remains to express the joint equilibrium equations in terms of the joint displacements and rotations, and this is accomplished with the aid of the slope–deflection equations. This step in the analysis is lengthy, but straightforward, and the algebraic effort is reduced with the use of finite difference operators. The results of this computation are six finite difference equations in terms of the displacements and rotations of the (m, n)th joint and the six joints adjacent to it. By expressing five of the displacement and rotation quantities in terms of the radial displacements $\underline{w}_{m,n}$, these six equations can be reduced to one finite difference equation in terms of normal joint displacements alone. Symbolically,

$$\mathscr{L}\underline{w}_{m,n} = 0 \tag{33}$$

where $\mathscr{L}$ is a 12th order finite difference operator and is omitted here in the interest of brevity.

The above finite difference equation admits periodic eigensolutions in the form

$$\underline{w}_{m,n} = \sin \mu m \sin \nu n \tag{34}$$

In Fig. 7 the curves shown are constructed by normalizing the value of the critical buckling load predicted by the discrete analysis with respect to the prediction of the equivalent shell analysis (23) and plotting this ratio for given values of GJ/EI, $\sin \alpha/2$, and L/r_g. The value of GJ/EI has been selected as 0·769 to correspond to beams of solid or hollow circular cross section such that $J/I = 2$ and the Poisson's ratio of the beam material is taken to be 0·3. The insert of Fig. 7 depicts the relationship of the angle α to the length parameters, L and R, such that $\sin \alpha/2 = L/2R$ and hence the critical parameter of continuum theory can be restated as $L^2/r_gR = 2(L/r_g) \sin \alpha/2$. Several curves for constant values of $L/\sqrt{(r_gR)}$ are cross-plotted in Fig. 7.

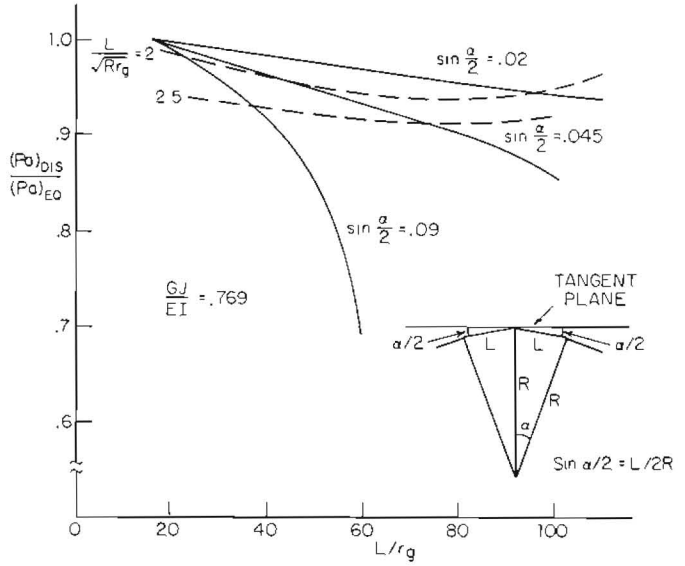

FIG. 7. Buckling of a shallow reticulated spherical section under external pressure (rigid joints).

A rough indication of the validity of the equivalent shell analysis can be obtained from the following discussion. When $L/\sqrt{(r_gR)}$ is about 2, the predictions of equivalent shell theory are 3–6 per cent higher than the actual buckling load predicted by the discrete

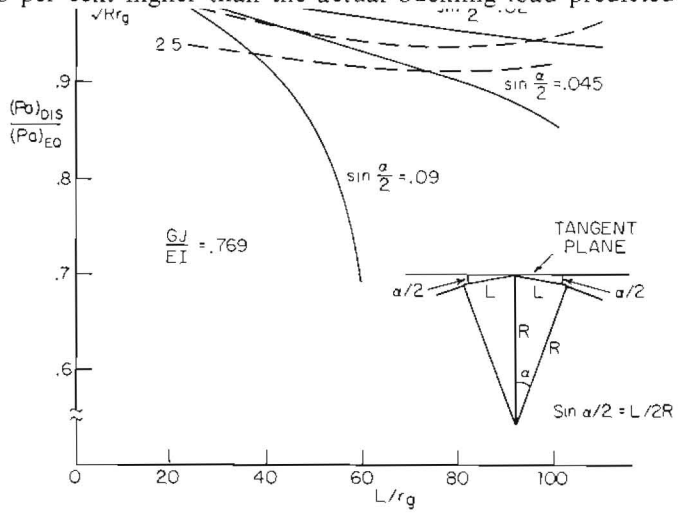

FIG. 7. Buckling of a shallow reticulated spherical section under external pressure (rigid joints).

A rough indication of the validity of the equivalent shell analysis can be obtained from

It should be explained that another important source of degradation of buckling strength is from geometric imperfections, that is, departures from the geometry of the perfect structure. In the range in which an equivalent shell analysis is approximately applicable for the rigidly jointed structure these effects can be treated just as they have been for shell theory [15]. They are not considered in this study.

The discontinuities in slope between the pairs of members described above are defined as follows

$$\theta_1^* = \theta_1(0) - \theta_4(L), \qquad \theta_2^* = \theta_2(0) - \theta_5(L), \qquad \theta_3^* = \theta_6(0) - \theta_3(L). \tag{36}$$

The previous equations (24) relating the rotations at the member ends to the joint rotations must now be modified to include the effects of the relative rotations of the member pairs. fn matrix form these modifications are

$$\Theta = B^* \Gamma^*_{m,n}. \tag{37}$$

Where Θ is a (6×1) matrix containing the values of the slopes at the ends of the members, $\Gamma^*_{m,n}$ is a (5×1) matrix containing the average values of the slopes at a joint [defined in the same way as in equation (8)] and the discontinuity factors, and B^* is a (6×5) matrix dependent on the geometric properties of the grid. They are given by

$$\Theta = [\theta_1(0), \theta_2(0), \theta_6(0), \theta_4(0), \theta_5(0), \theta_3(0)]$$

$$\Gamma^*_{m,n} = [\underline{\gamma}_{m,n}, \underline{\theta}_{m,n}, \theta_1^*, \theta_2^*, \theta_3^*]$$

$$B^* = \begin{bmatrix} 0 & 1 & 1/2 & 0 & 0 \\ -\sqrt{3}/2 & 1/2 & 0 & 1/2 & 0 \\ \sqrt{3}/2 & 1/2 & 0 & 0 & 1/2 \\ 0 & 1 & -1/2 & 0 & 0 \\ -\sqrt{3}/2 & 1/2 & 0 & -1/2 & 0 \\ \sqrt{3}/2 & 1/2 & 0 & 0 & -1/2 \end{bmatrix}.$$

If the effects of the rotational springs on the internal virtual work of the system are taken into account, it can be shown by proceeding exactly as in the analysis of the spherical segment with rigid joints, that the member equations remain the same but now there are three more joint equilibrium equations in addition to (30). Again, buckling is associated

Where Θ is a (6×1) matrix containing the values of the slopes at the ends of the members, $\Gamma^*_{m,n}$ is a (5×1) matrix containing the average values of the slopes at a joint [defined in the same way as in equation (8)] and the discontinuity factors, and B^* is a (6×5) matrix dependent on the geometric properties of the grid. They are given by

$$\Theta = [\theta_1(0), \theta_2(0), \theta_6(0), \theta_4(0), \theta_5(0), \theta_3(0)]$$

$$\Gamma^*_{m,n} = [\underline{\gamma}_{m,n}, \underline{\theta}_{m,n}, \theta_1^*, \theta_2^*, \theta_3^*]$$

$$B^* = \begin{bmatrix} 0 & 1 & 1/2 & 0 & 0 \\ -\sqrt{3}/2 & 1/2 & 0 & 1/2 & 0 \\ \sqrt{3}/2 & 1/2 & 0 & 0 & 1/2 \\ 0 & 1 & -1/2 & 0 & 0 \\ -\sqrt{3}/2 & 1/2 & 0 & -1/2 & 0 \\ \sqrt{3}/2 & 1/2 & 0 & 0 & -1/2 \end{bmatrix}.$$

If the effects of the rotational springs on the internal virtual work of the system are

A typical curve showing the effects of non-rigid joints is given in Fig. 8 along with a curve for the same structure with rigid joints. In both instances the buckling loads have been normalized by the prediction (23) of the equivalent shell theory for the rigidly jointed structure.

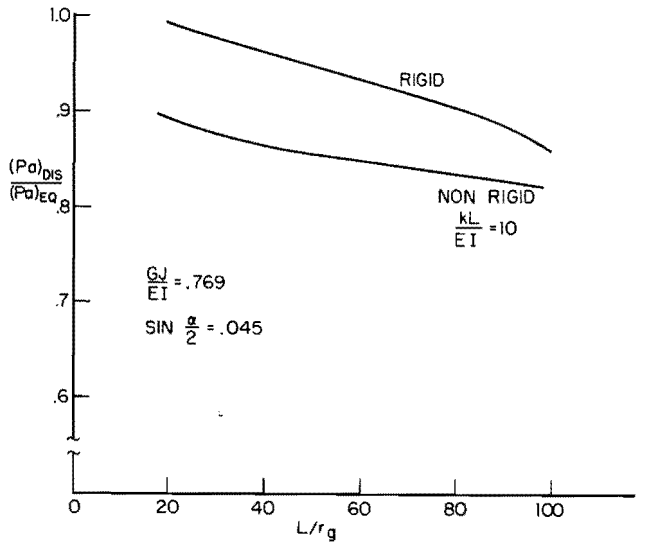

FIG. 8. Buckling of a shallow reticulated spherical section under external pressure (non-rigid joints).

It is recalled that the simple formula, equation (20), showing the effects of non-rigid joints on the beam-spring model, was derived for the range where the wavelengths of buckling were "long" compared to the member lengths and the axial member loads were "small" compared to the Euler load. It should be interesting to see if this formula is approximately correct when applied to the spherical section with non-rigid joints in the same range. A number of calculations have been made, and it has been found that the simple model gives an excellent approximation to the effect of non-rigid joints on the buckling

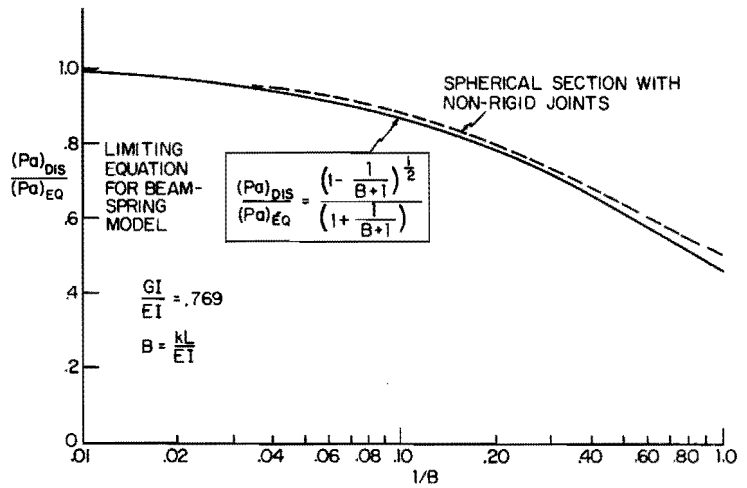

FIG. 9. Effects of non-rigid joints on buckling: comparison of the predictions for the beam-spring model with the predictions for the spherical section.

behavior of the spherical section. Some results are presented in Fig. 9 for the case of sin $\alpha/2 = 0{\cdot}005$ and $L/r_g = 40$. A limited numerical investigation shows similar agreement for other combinations of L/r_g and sin $\alpha/2$ so long as $L/\sqrt{(r_g R)}$ is less than about unity.

BUCKLING OF AN INFINITE RETICULATED CYLINDER UNDER AXIAL COMPRESSION

In this section results are reported for an equivalent shell analysis and a discrete analysis for an infinite reticulated cylinder, with an equilateral triangle grid and rigid joints, subject to axial compression. Each beam in the cylinder is of length L and each joint is a distance R from the longitudinal cylinder axis. The gridwork is loaded by a total axial force, as depicted in Fig. 10, which corresponds to an axial pre-buckling load F in each of the longitudinal

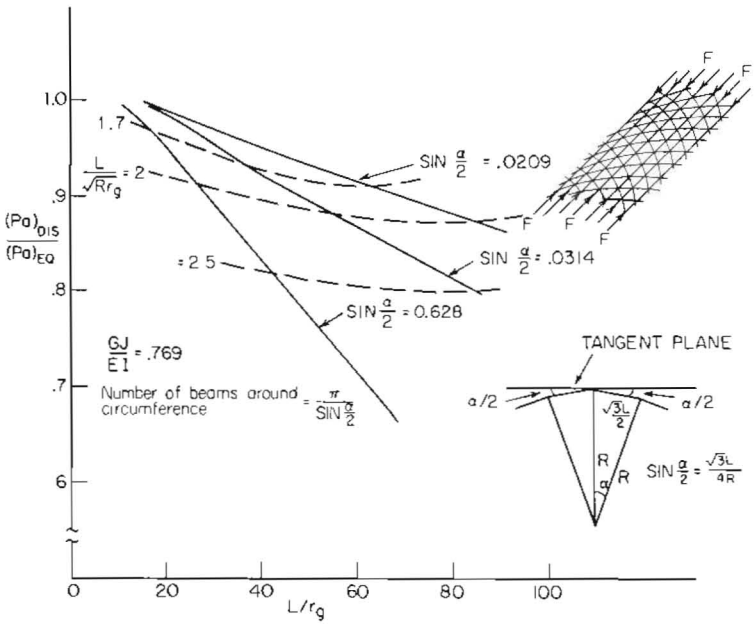

FIG. 10. Buckling of a reticulated cylinder under axial compression.

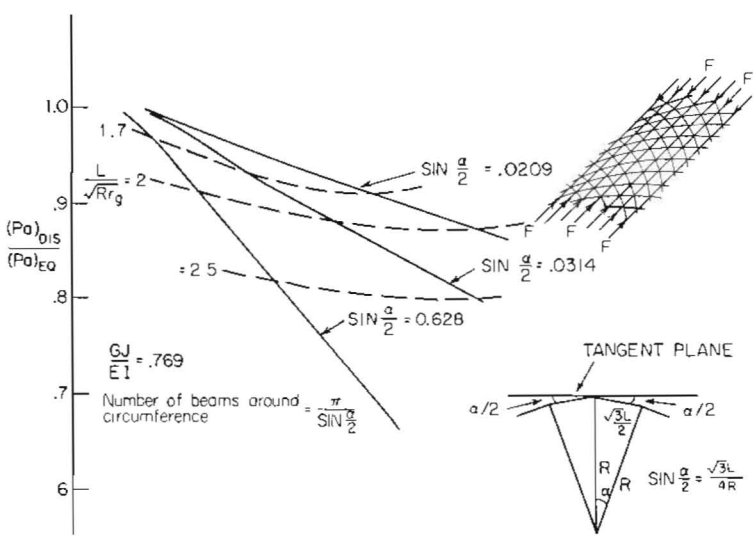

In the equivalent shell analysis, the loading applied to the cylinder as described above is replaced by a uniform force per unit circumference N where $N = 2F/\sqrt{(3)}L$, and the stiffness properties of the equilateral triangle grid are the same as those used in the analysis of the spherical section and given by equation (21). The classical buckling load of an isotropic cylindrical shell is given by the well-known formula

$$N_c = \frac{2}{R}[D_e(Et)_e]^{\frac{1}{2}} \tag{40}$$

The non-dimensional parameter for the axial load in the longitudinal members is given by

$$\left(\frac{P_a L^2}{EI}\right) = \frac{L^2}{r_g R}\left[\frac{3}{2}\left(3+\frac{GJ}{EI}\right)\right]^{\frac{1}{2}} \tag{41}$$

where $P_a \equiv F$; and in this problem also, the buckle wavelengths are on the order of $\sqrt{(r_g R)}$.

The discrete analysis of the cylinder is carried out along the same lines as has already been outlined in the spherical section. The buckling deformation of the structure can be characterized by specifying three displacements and three rotations at each joint. The length parameters of the grid L and R are related to the angle α defined in Fig. 10 by $\sin \alpha/2 = \sqrt{(3)}L/4R$. Buckling is associated with bifurcation from the pre-buckling state and resulting eigenvalue equation is of the form

$$F\left(\frac{P_a L^2}{EI}, \mu, \nu, \frac{L}{r_g}, \sin\frac{\alpha}{2}, \frac{GJ}{EI}\right) = 0$$

where μ and ν are the wave numbers associated with the eigenmodes $\underline{w}_{m,n} = \sin \mu m \sin \nu n$.

As expected, the eigenvalues predicted by the discrete theory for given pairs of axial and circumferential wavelengths are essentially identical to the corresponding eigenvalues from the equivalent shell theory as long as the wavelengths are sufficiently long compared to the member lengths. When the parameter $L/\sqrt{(r_g R)}$ is less than about unity the critical eigenvalues from the two analyses are in substantial agreement and equation (41) is valid. However, when $L/\sqrt{(r_g R)}$ is greater than unity the critical eigenvalue of the discrete analysis

$$\left(\frac{P_a L^2}{EI}\right) = \frac{L^2}{r_g R}\left[\frac{3}{2}\left(3+\frac{GJ}{EI}\right)\right]^{\frac{1}{2}} \tag{41}$$

where $P_a \equiv F$; and in this problem also, the buckle wavelengths are on the order of $\sqrt{(r_g R)}$.

The discrete analysis of the cylinder is carried out along the same lines as has already been outlined in the spherical section. The buckling deformation of the structure can be characterized by specifying three displacements and three rotations at each joint. The length parameters of the grid L and R are related to the angle α defined in Fig. 10 by $\sin \alpha/2 = \sqrt{(3)}L/4R$. Buckling is associated with bifurcation from the pre-buckling state and resulting eigenvalue equation is of the form

$$F\left(\frac{P_a L^2}{EI}, \mu, \nu, \frac{L}{r_g}, \sin\frac{\alpha}{2}, \frac{GJ}{EI}\right) = 0$$

where μ and ν are the wave numbers associated with the eigenmodes $\underline{w}_{m,n} = \sin \mu m \sin \nu n$.

As expected, the eigenvalues predicted by the discrete theory for given pairs of axial and circumferential wavelengths are essentially identical to the corresponding eigenvalues from the equivalent shell theory as long as the wavelengths are sufficiently long compared

OPTIMIZATION OF A RETICULATED STRUCTURE

A light weight design of a reticulated structure will favor long slender members and a proper optimization analysis will necessarily have to be discrete. To illustrate this we have choseu to optimize the equilateral triangular grid of a shallow reticulated spherical shell with rigid joints. Each member of the grid is taken to have a solid circular cross-section; and in addition, the radius of the spherical segment R and the effective buckling pressure per unit area p_c are regarded as being specified. The structure is to be designed against buckling by selecting the member length L and the radius of gyration of the member cross-section r_g such that the weight is optimized.

The weight per unit area W is

$$W = 8\pi\sqrt{(3)}\rho_0 r_g^2/L$$

where ρ_0 is the material density. The following convenient non-dimensional parameter W^* will be minimized subject to the buckling constraint:

$$W^* \equiv \frac{W}{16\pi\sqrt{(3)}R\rho_0} = \frac{L/2R}{(L/r_g)^2}. \tag{42}$$

Separate calculations for the optimum values of L/r_g and $L/2R = \sin\alpha/2$ which produce the optimum weight are carried out, first using an equivalent shell analysis and then using the discrete analysis.

The critical value of the pre-buckling loads in every member is given by

$$\left(\frac{P_a L^2}{EI}\right)_{\text{crit}} = \frac{(L/r_g)^4}{16\sqrt{(3)}\pi\sin\alpha/2}\left(\frac{p_c}{E}\right). \tag{43}$$

The critical buckling pressure of the equivalent shell model of the reticulated shell, obtained from equation (22), is given by the expression

$$\frac{p_c}{E} = \frac{8\pi(r_g/R)^2}{L/r_g}\left[2\left\{3+\frac{2G}{E}\right\}\right]^{\frac{1}{2}} \tag{44}$$

where ρ_0 is the material density. The following convenient non-dimensional parameter W^* will be minimized subject to the buckling constraint:

$$W^* \equiv \frac{W}{16\pi\sqrt{(3)}R\rho_0} = \frac{L/2R}{(L/r_g)^2}. \tag{42}$$

Separate calculations for the optimum values of L/r_g and $L/2R = \sin\alpha/2$ which produce the optimum weight are carried out, first using an equivalent shell analysis and then using the discrete analysis.

The critical value of the pre-buckling loads in every member is given by

$$\left(\frac{P_a L^2}{EI}\right)_{\text{crit}} = \frac{(L/r_g)^4}{16\sqrt{(3)}\pi\sin\alpha/2}\left(\frac{p_c}{E}\right). \tag{43}$$

The critical buckling pressure of the equivalent shell model of the reticulated shell, obtained from equation (22), is given by the expression

The minimum value of W^* is found subject to the constraint (45). The optimum member properties are given by

$$\frac{r_g}{R} = \left[\frac{\beta(p_c/E)^2}{192\left(\frac{2}{3}\left(3+\frac{2G}{E}\right)\right)^{\frac{1}{2}}}\right]^{\frac{1}{3}} \tag{46}$$

$$\frac{L}{r_g} = \frac{8\pi}{(p_c/E)}\left[2\left(3+\frac{2G}{E}\right)\right]^{\frac{1}{2}}\left(\frac{r_g}{R}\right)^2 \tag{47}$$

and

$$\sin\frac{\alpha}{2} = \frac{1}{2}\left(\frac{L}{r_g}\right)\left(\frac{r_g}{R}\right). \tag{48}$$

Use is now made of the eigenvalue equation of the discrete analysis which was derived in the third section and, in functional notation, is given by

$$F\left(\frac{P_aL^2}{EI}, \mu, \nu, \frac{L}{r_g}, \sin\frac{\alpha}{2}, \frac{GJ}{EI}\right) = 0.$$

This equation is used with the previous expression for W^* and (43), in which $(P_aL^2/EI)_c$ is related to the prescribed pressure, to locate the optimum values of L/r_g and $\sin\alpha/2$ associated with the minimum weight (GJ/EI is again chosen to be 0·769). A straightforward search procedure was used to determine the optimum properties.

A selection of optimum properties determined by the two different analyses have been tabulated in Table 1 for the following values of the parameter p_c/E, $6{\cdot}67\times10^{-7}$, 10×10^{-7} and $13{\cdot}3\times10^{-7}$ which typify loads encountered by steel roof structures under snow loading.

TABLE 1. OPTIMUM PROPERTIES FOR A SHALLOW SECTION OF A RETICULATED SPHERICAL SHELL SUBJECT TO PRESCRIBED NORMAL LOADING

		Equivalent shell analysis			
p_{crit}/E $\times10^{-7}$	$\sin\frac{\alpha}{2}$	$\frac{L}{r_g}$	W^* $\times10^{-7}$	β	$\frac{1}{\pi^2}\left(\frac{P_aL^2}{EI}\right)_{exact}$
6·67	0·0130	191	3·56	0·8	0·74
6·67	0·0139	200	3·48	0·9	0·82
6·67	0·0148	208	3·43	1·0	0·90
10	0·0140	176	4·52	0·8	0·74
10	0·0150	184	4·46	0·9	0·82
10	0·0162	193	4·34	1·0	0·91
13·3	0·01485	166	5·39	0·8	0·73
13·3	0·01595	174	5·26	0·9	0·82
13·3	0·0170	181	5·16	1·0	0·91
		Discrete analysis			
6·67	0·0182	231	3·42	—	1·22
10	0·0210	217	4·47	—	1·23
13·3	0·0216	202	5·23	—	1·22

With regard to the equivalent shell predictions, it can be noted at once that the more conservative the choice of β (we have arbitrarily chosen $\beta = 0{\cdot}8$, $0{\cdot}9$ and $1{\cdot}0$), the heavier the structure will be. To assess the reliability of this very crude analysis the actual buckling loads have been calculated using the predicted optimum value of L/r_g and $\sin \alpha/2$. Typically the actual axial member load at buckling is found to be as much as 10 per cent lower than what was designed for using the equivalent shell analysis. The optimum values of L/r_g and $\sin \alpha/2$ predicted by the discrete analysis are about 20–30 per cent higher than those predicted by the equivalent shell analysis for the pressures considered. Moreover the loads in the members of the optimum structure at buckling are roughly 20 per cent higher than the Euler load of a simply supported column. In spite of the discrepancies between the two analyses, it is interesting to note that both predict essentially the same minimum weight.

CLOSURE

Buckling results for reticulated shell structures in the form of bifurcation from a uniform pre-buckling state serve the same purpose as their counterpart solutions in continuum shell theory. Namely, they provide upper estimates for the load carrying capacity of the structure. These estimates will be lowered by many factors such as nonuniformities due to edge conditions, nonuniformity of loading and imperfections of various sorts. In particular, without further studies, both theoretical and experimental, it must be assumed the imperfections will play at least the same degrading role in the buckling of reticulated shell structures as they have been found to do in regular shell structures.

Based on the results for the three reticulated structures studied here, the following generalizations seem reasonable for shell structures of this type. For a rigid jointed structure, the equivalent shell analysis should be substantially correct as long as the maximum axial load in any member does not exceed about 70 per cent of the simple-support Euler load and at this value the equivalent shell predictions should be less than 10 per cent too high. The effect of non-rigid joints (but perfect geometry), in the range in which the rigid jointed structure is adequately modeled by the equivalent shell theory is indicated by the formula

$$\frac{(P_a)_c}{(P_a)_{\text{equiv}}} = \frac{[1-1/(B+1)]^{\frac{1}{2}}}{1+1/(B+1)}$$

where $(P_a)_c/(P_a)_{\text{equiv}}$ is the ratio of the buckling load of the structure with non-rigid joints

CLOSURE

Buckling results for reticulated shell structures in the form of bifurcation from a uniform pre-buckling state serve the same purpose as their counterpart solutions in continuum shell theory. Namely, they provide upper estimates for the load carrying capacity of the structure. These estimates will be lowered by many factors such as nonuniformities due to edge conditions, nonuniformity of loading and imperfections of various sorts. In particular, without further studies, both theoretical and experimental, it must be assumed the imperfections will play at least the same degrading role in the buckling of reticulated shell structures as they have been found to do in regular shell structures.

Based on the results for the three reticulated structures studied here, the following generalizations seem reasonable for shell structures of this type. For a rigid jointed structure, the equivalent shell analysis should be substantially correct as long as the maximum axial load in any member does not exceed about 70 per cent of the simple-support Euler load and at this value the equivalent shell predictions should be less than 10 per cent too high. The effect of non-rigid joints (but perfect geometry), in the range in which the rigid jointed structure is adequately modeled by the equivalent shell theory is indicated by the formula

[8] F. BLEICH, *Buckling Strength of Metal Structures*, pp. 210–211. McGraw-Hill (1952).
[9] W. MERCHANT and A. H. SALEM, The use of stability functions in the analysis of rigid frames. *Proc. Sixth Congr. IABSE*, pp. 457–460. Stockholm (1960).
[10] R. K. LIVESLY and D. B. CHANDLER, *Stability Functions for Structural Frameworks*. Manchester University Press (1956).
[11] L. M. MILNE-THOMSON, *The Calculus of Finite Differences*, pp. 31–34. MacMillan (1933).
[12] H. LEVY and F. LESSMAN, *Finite Difference Equations*. Pitman (1959).
[13] B. BUDIANSKY, P. SEIDE and P. A. WEINBERGER, The buckling of a column on equally spaced deflectional and rotational springs, NACA Technical Note 1519 (1948).
[14] J. D. RENTON and L. G. JAEGER, Fine triangular mesh gridworks, (to be published).
[15] J. W. HUTCHINSON, Imperfection sensitivity of externally pressurized spherical shells, *J. appl. Mech.* **34**, 49–55 (1967).

(*Received* 17 *June* 1969; *revised* 17 *September* 1969)

Абстракт—Дается анализ устойуивости некоторых конструкций сетчатых оболочек, путем использования так приближенного анализа оболочек, как и анализа дискретных систем, который, в основном, является точным. Рассматриваются следующие конструкции: бесконеуная сетчатая балка, сжимаемая осевым давлением и лежащая на пружинах, расположенных в равном расстоянии, пологая часть сетчатой сферы с равносторонной трехугольной сеткой, подверженная нормальной нагрузке и бесконечная, цилиндрическая оболочка с равносторонной трехугольной сеткой, подверженная осевому сжатию. Используееся анализ дискретных систем с целью сравнения точности условий анализа эквивалентных оболочек. Нагрузка выпучивания, расчитана на основе эквивалентного анализа оболочек, является неконсервативной, когда как длина волны деформации выпучивания равна порядку длины элемента, или когда осевая нагрузка в элементе при потере устойчивости равна порядку величины нагрузки выпучивания Эйлера для свободно опертой колонны. Исследуется эффект нагрузки выпучивания, уменьшающий жесткость соединений так для модели балка-пружина, как и для сферической сетчатой оболочки. На конец, иллюстрируется важность анализа дискретных систем путем определения оптимальных свойств пологой части сетчатой сферы, подверженной действию нормальной нагрузки и расчитанной с учетом выпучивания.